Supporting Information

Engineering Hierarchical Snowflake Flakes Multi-Metal Selenide Catalysts Anchored on Ni Foam for High-Efficiency Stable Overall Water Splitting

Enze Fan[a], Shuangqi Zhou[a], Hanwei Zhao[a], Jianxin Ran[a], Zhuanfang Zhang[b,*], Guohua Dong[a,*], Wenzhi Zhang[a], Yu Zang[c], Ming Zhao[a], Dong-Feng Chai[a], Xiaoming Huang[b]

[a] College of Chemistry and Chemical Engineering, Qiqihar University, Qiqihar 161006, PR China.

[b] Center of Teaching Experiment Management Equipment, Qiqihar University, Qiqihar 161006, PR China.

[c] College of Materials Science and Engineering, Heilongjiang Provincial Key Laboratory of Polymeric Composite Materials, Qiqihar University, Qiqihar 161006, PR China.

*Corresponding author. E-mail: zzfhao2014@163.com; ghdong@qqhru.edu.cn.

Number of Pages: 26

Number of Figures: 14

Number of Tables: 3

Experimental Section:

1. Materials

All chemicals were purchased and used without any further purification. Cobaltous acetate ($C_4H_6CoO_4 \cdot 4H_2O$, Tianjin Guangfu Fine Chemical Research Institute), phosphotungstic acid ($H_3PW_{12}O_{40} \cdot xH_2O$, Tianjin Guangfu), selenium powder (Beijing Chemical Plant), potassium hydroxide (KOH, Tianjin Kaitong Chemical Reagents Co., Ltd.), ethanol absolute (C_2H_5OH, Tianjin Tianli Chemical Reagent Co., Ltd.), hydrochloric acid (HCl, Nanjing Chemical Reagent Co., Ltd.), acetone (C_3H_6O, 99.7%, Nanjing Reagent), Ni foam (NF, Kunshan Jiayisheng Electronics Co., Ltd.), 5% Pt/C (Shanghai Aladdin Biochemical Technology Co., Ltd.), and RuO_2 (Aladdin). Deionized (DI) water was used throughout the experimental processes.

2. Synthesis of W-CoO/NF Precursor

A piece of NF (2 cm × 4 cm) was immersed in acetone, 10wt% HCl, DI water and ethanol respectively, and ultrasonic treatment was carried out for 15 min to remove residual organic matter and eliminate oxides on the surface of NF. Afterward, a piece of treated NF was vertically placed into the inner lining of 50 mL stainless steel reactor, and 40 mL of homogeneous solution was added, containing $H_3PW_{12}O_{40}$ (0.125 mmol) and $C_4H_6CoO_4$ (1.73 mmol). Subsequently, the PTFE stainless steel autoclave was sealed and heated at 180 ℃ for 8 h. After the reaction, the NF substrate was cleaned with DI water until the surface was free of impurities, the sample was collected and vacuum dried at 60 ℃, and it was named W-CoO/NF.

3. Synthesis of W-CoSe300/NF

Using the prepared W-CoO/NF as a precursor, W-CoSe300/NF can be obtained by a one-step high temperature selenization process. The details are as follows: W-CoO/NF and selenium powder were placed in a tube furnace, selenium powder in the upstream and W-CoO/NF in the downstream, the heating rate was 2 ℃ min^{-1}, and calcined at 300 ℃ in H_2/Ar atmosphere for 3 h. Naturally cooled to room temperature, the W-CoSe300/NF with snowflake flakes structure was obtained.

As a comparison, a series of W-CoO/NF precursors with varying tungsten doping levels were synthesized by controlling the ratio of added M ($H_3PW_{12}O_{40}$) and M ($C_4H_6CoO_4$) to be 0.024, 0.048, 0.072, 0.096, and 0.120, and the corresponding W-CoSe300/NF electrocatalysts were prepared.

4. Physical Characterizations:

The microstructure and morphology of the electrocatalyst prepared in this study were tested by Hitachi S-4300 scanning electron microscope (SEM) and energy dispersive X-ray spectrometer (EDS) at an accelerated voltage of 20 kV. In order to observe the microstructure of the materials on the nanoscale, the samples were tested with Hitachi H-7650 transmission electron microscope (TEM) at an accelerated voltage of 100 kV. High-resolution transmission electron microscopy (HRTEM) images of the samples were obtained by Tecnai G2 F20 transmission electron microscope produced by FEI Company in the United States at 200 kV acceleration voltage. In order to analyze the chemical components of the prepared electrocatalyst and the corresponding crystal phase structure, the phase characterization of the sample

was tested by Bruker-AXS (D8) X-ray diffractometer (XRD). In order to explore the valence state and electronic structure of the material surface, the prepared electrocatalyst was tested by VG ESCALAB MK X-ray photoelectron spectrometer produced by VG Company in UK. All electrochemical data were determined using the CHI660E electrochemical workstation.

5. Electrochemical Measurements:

All electrochemical tests were performed in 1.0 M KOH (pH ≈ 14) aqueous solution at room temperature. The three-electrode system was connected with an electrochemical workstation (CHI 660E, Shanghai Chenhua), in which the reference electrode was Hg/HgO and the electrode was graphite rod. All linear sweep voltammetry (LSV) curves were measured at a scan rate of 5 mV s^{-1} without IR compensation. Working potentials were converted with respect to reversible hydrogen electrode (RHE) according to the following equation:

$$E\ (RHE) = E\ (Hg/HgO) + 0.098\ (V) + 0.059 \times pH$$

For the LSV curve of oxygen evolution reaction (OER), the overpotential (η) of each electrode material was calculated according to the following equation:

$$\eta = E\ (RHE) - 1.23\ (V)$$

The Tafel slope was calculated according to the following equation:

$$\eta = b \log | j | + a$$

Here, j represents the current density, a is a constant, and b represents the Tafel slope.

To further evaluate the electrocatalytic activity under different overpotentials (η), the turnover frequency (TOF, s^{-1}) of the electrode materials was calculated in the

following two steps: (I) calculate the active sites n (mol); (II) calculate the TOF value (s^{-1}). The number of active sites is determined by CV curves, which collected from CV measurements conducted at a scan rate of 50 mV s^{-1} in 1.0 M phosphate buffer solution (PBS, pH ≈ 7). Then, the absolute components of the voltammetric charges (cathodic and anodic) reported during a single blank test is added. Assuming that both reduction and oxidation are one-electron processes, the maximum of n can be calculated using the following formula:

$$n = Q/\alpha F \qquad (4)$$

Then, TOF can be calculated with the following formula:

$$TOF = I/\alpha F n \qquad (5)$$

Where α is the number of transferred electrons corresponding to a half reaction that produces 1 mol target product or consumes 1 mol target reactant (for HER in 1.0 M KOH, α = 2), Q is the voltammetric charge, F is the Faraday constant (96485 C mol^{-1}), I is the current (A) during the linear sweep measurement and n is the number of active sites (mol).

Electrochemical impedance spectroscopy (EIS) was carried out at an overpotential of current density at 10 mA cm^{-2} with a frequency range from 0.01 Hz to 100 kHz.

The double-layer capacitance (C_{dl}) was obtained by cyclic voltammetry (CV) curves at different scanning rates (20, 40, 60, 80, and 100 mV s^{-1}) to assess the electrochemical active surface area (ECSA) of the catalysts.

The stability of the electrocatalyst was measured by chronoamperometry and cyclic voltammetry.

Figure and Table Captions:

Fig. S1. (a) W-CoSe200/NF， (b) W-CoSe300/NF， (c) W-CoSe400/NF SEM with different scanning multiples of (a1)W-CoSe200/NF, (b1) W-CoSe300/NF, (c1) W-CoSe400/NF.

Fig. S2. EDS mapping of W-CoSe300/NF electrocatalyst and corresponding elemental mass percentage content.

Fig. S3. (a) HER polarization curves (b) Tafel (c) EIS and (d) OER polarization curves (e) Tafel (f) EIS of W-CoO/NF precursors with different reaction times.

Fig. S4. (a) HER polarization curves (b) Tafel (c) EIS and (d) OER polarization curves (e) Tafel (f) EIS of W-CoO/NF precursors with different solvent ratios.

Fig. S5. (a) HER polarization curves (b) Tafel (c) EIS and (d) OER polarization curves (e) Tafel (f) EIS of W-CoO/NF precursors with different reaction temperatures.

Fig. S6. (a) HER polarization curves (b) Tafel (c) EIS and (d) OER polarization curves (e) Tafel (f) EIS of W-CoO/NF precursors with different reaction solute mass ratio.

Fig. S7. HER-CV of (a) W-CoO/NF (b) W-CoSe200/NF (c) W-CoSe300/NF and (d) W-CoSe400/NF at different sweep speeds.

Fig. S8. The turnover frequency (TOF) of W-CoSe300/NF electrocatalysts with different M ($H_3PW_{12}O_{40}$)/M ($C_4H_6CoO_4$) ratios and their corresponding cyclic voltammetry (CV) curves (in PBS solution, pH ≈ 7).

Fig. S9. LSV curves of W-CoSe200/NF, W-CoSe300/NF, and W-CoSe400/NF electrocatalyst normalized by ECSA.

Fig. S10. OER-CV of (a) W-CoO/NF (b) W-CoSe200/NF (c) W-CoSe300/NF and (d) W-CoSe400/NF at different sweep speeds.

Fig. S11. EIS Nyquist plots of W-CoSe300 electrocatalysts loaded on different conductive substrates.

Fig. S12. Stability tests of W-CoSe300/GCE and W-CoSe300/NF electrocatalysts under HER and OER overpotentials (GCE = glassy carbon electrode).

Fig. S13. OWS performance of W-CoSe300/GCE (GCE = glassy carbon electrode) and W-CoSe300/NF electrocatalysts: (a) LSV curves, (b) electrochemical stability test.

Fig. S14. Characterization analysis of the W-CoSe300/NF electrocatalyst after OER stability testing: (a) SEM image, (b) TEM image, (c, d) XPS spectra.

Table S1. The comparison for HER performance of W-CoSe300/NF synthesized in this work and recently reported catalysts.

Table S2. The comparison for OER performance of W-CoSe300/NF synthesized in this work and recently reported catalysts.

Table S3. The comparison for overall water splitting (OWS) performance of W-CoSe300/NF synthesized in this work and recently reported catalysts.

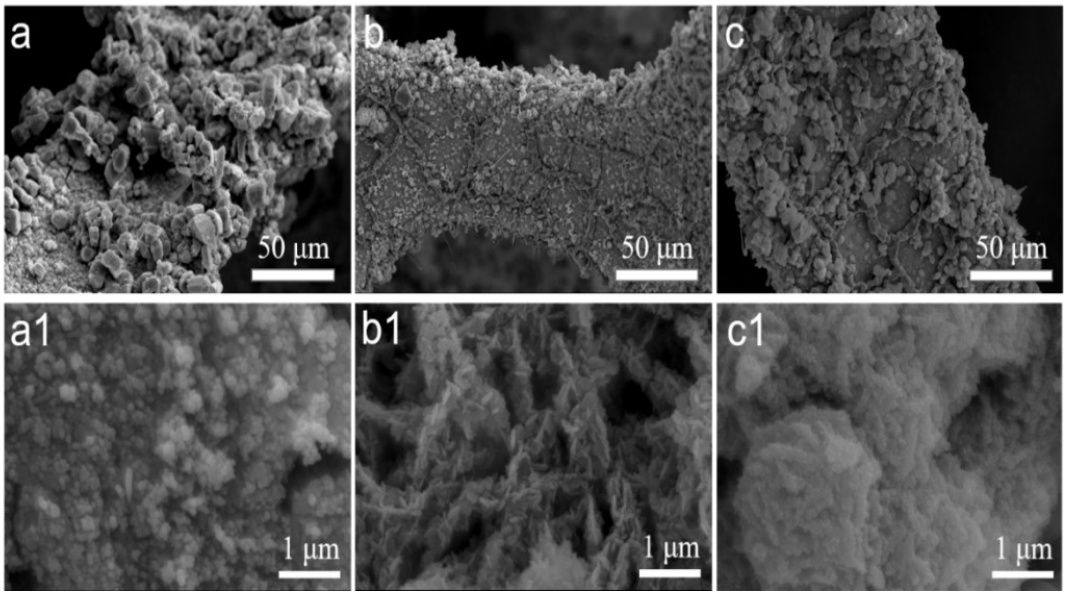

Fig. S1. (a) W-CoSe200/NF， (b) W-CoSe300/NF， (c) W-CoSe400/NF SEM with different scanning multiples of (a1)W-CoSe200/NF, (b1) W-CoSe300/NF, (c1) W-CoSe400/NF.

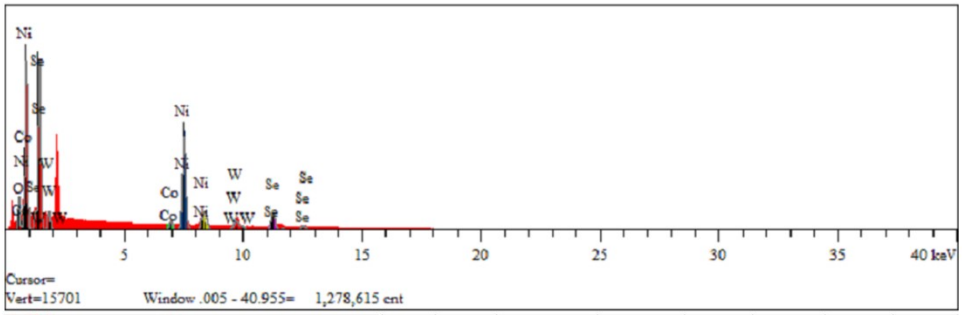

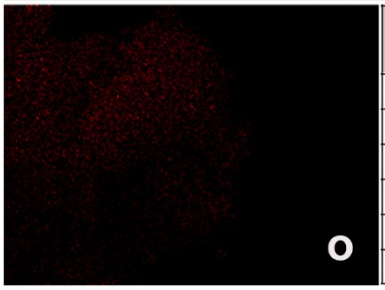

Elt.	Line	Intensity (c/s)	Conc	Units	Error 2-sig	MDL 3-sig	
O	Ka	2,493.47	8.026	wt.%	.166	.200	
Co	Ka	1,097.71	2.561	wt.%	.076	.088	
Ni	Ka	11,445.87	31.057	wt.%	.312	.385	
Se	Ka	2,332.53	32.069	wt.%	.678	.809	
W	La	1,703.25	26.288	wt.%	.658	.792	
			100.000	wt.%			Total

Fig. S2. EDS mapping of W-CoSe300/NF electrocatalyst and corresponding elemental mass percentage content.

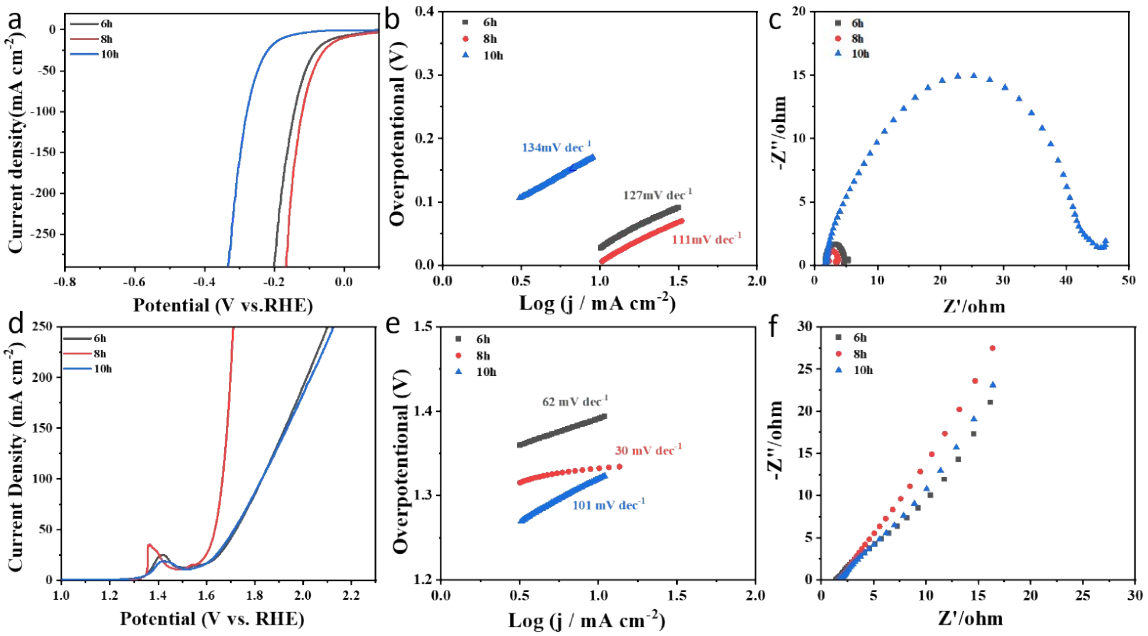

Fig. S3. (a) HER polarization curves (b) Tafel (c) EIS and (d) OER polarization curves (e) Tafel (f) EIS of W-CoO/NF precursors with different reaction times.

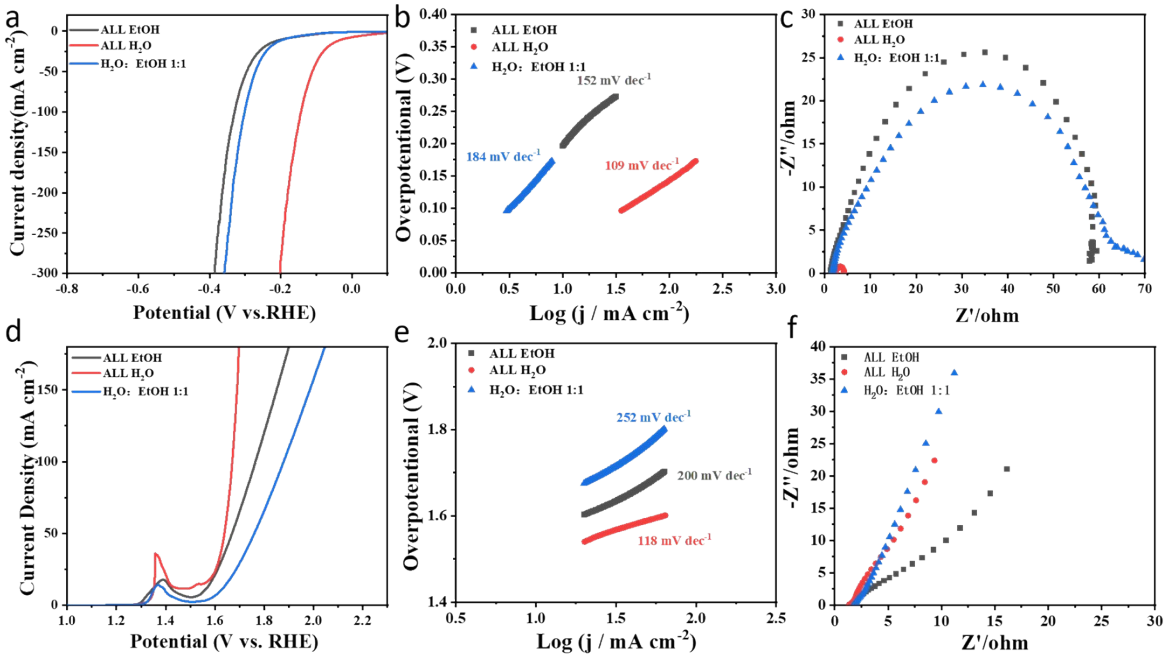

Fig. S4. (a) HER polarization curves (b) Tafel (c) EIS and (d) OER polarization curves (e) Tafel (f) EIS of W-CoO/NF precursors with different solvent ratios.

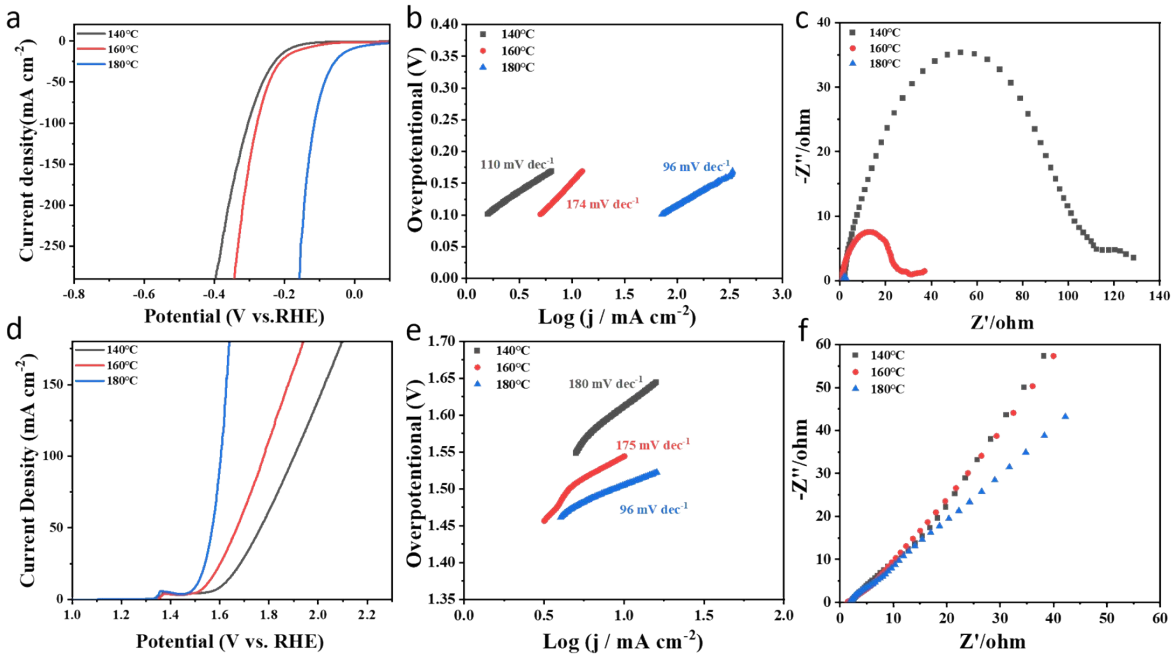

Fig. S5. (a) HER polarization curves (b) Tafel (c) EIS and (d) OER polarization curves (e) Tafel (f) EIS of W-CoO/NF precursors with different reaction temperatures.

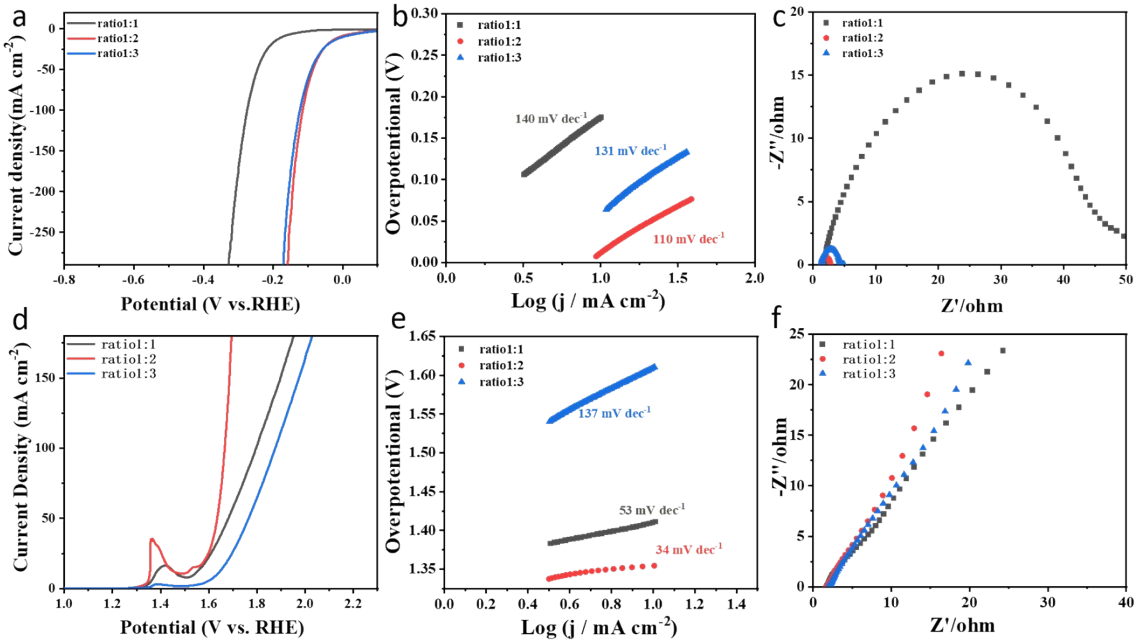

Fig. S6. (a) HER polarization curves (b) Tafel (c) EIS and (d) OER polarization curves (e) Tafel (f) EIS of W-CoO/NF precursors with different reaction solute mass ratio.

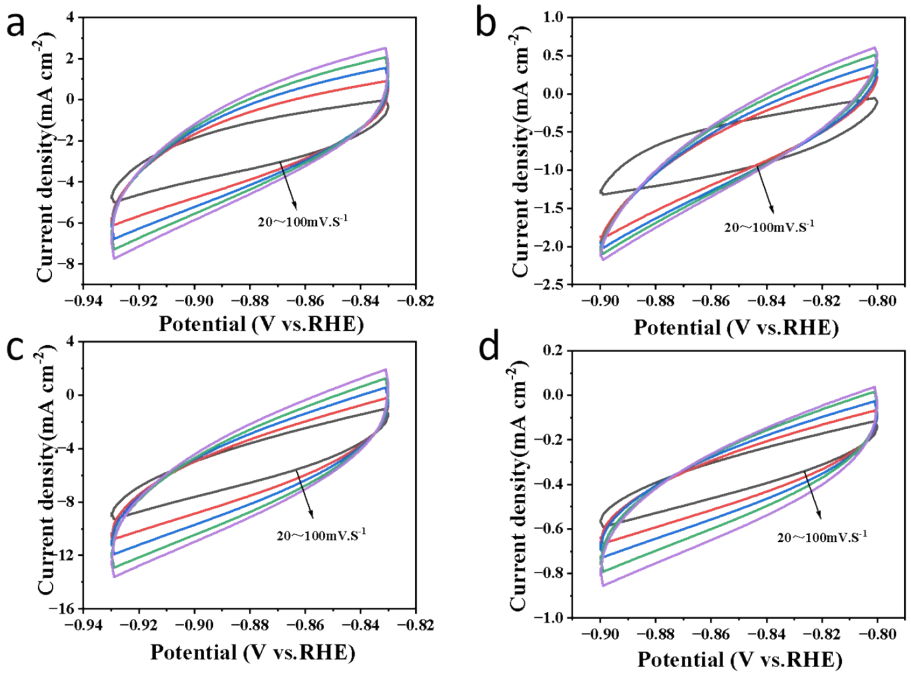

Fig. S7. HER-CV of (a) W-CoO/NF (b) W-CoSe200/NF (c) W-CoSe300/NF and (d) W-CoSe400/NF at different sweep speeds.

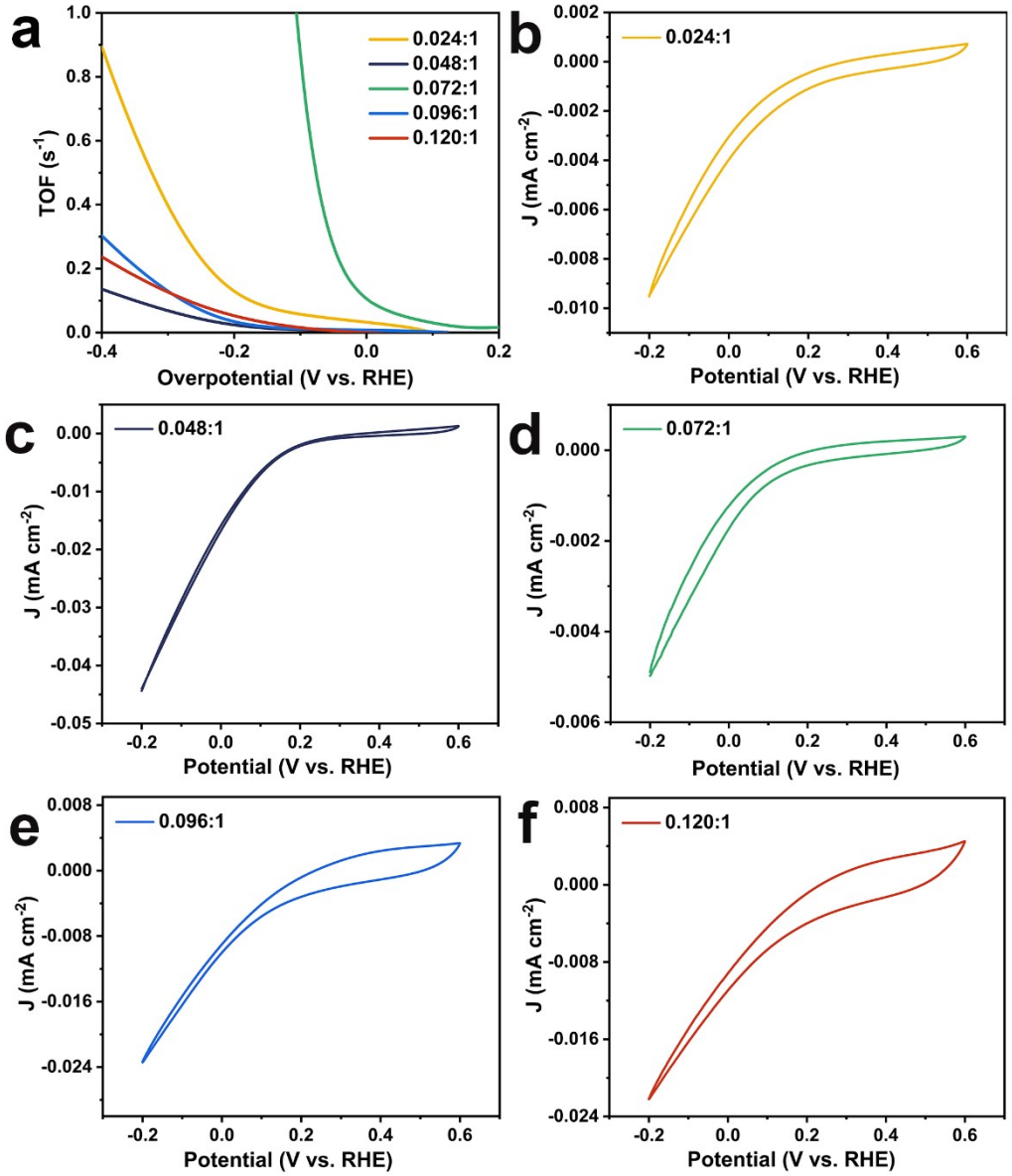

Fig. S8. The turnover frequency (TOF) of W-CoSe300/NF electrocatalysts with different M ($H_3PW_{12}O_{40}$)/M ($C_4H_6CoO_4$) ratios and their corresponding cyclic voltammetry (CV) curves (in PBS solution, pH ≈ 7).

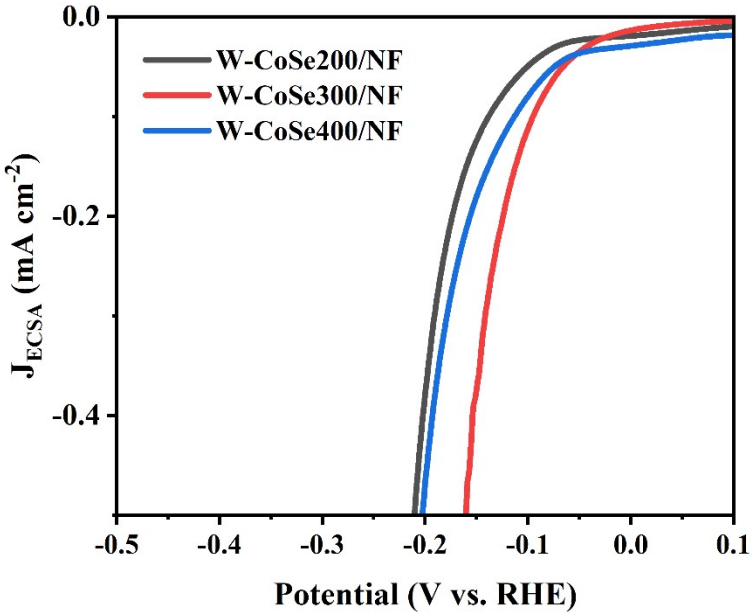

Fig. S9. LSV curves of W-CoSe200/NF, W-CoSe300/NF, and W-CoSe400/NF electrocatalyst normalized by ECSA.

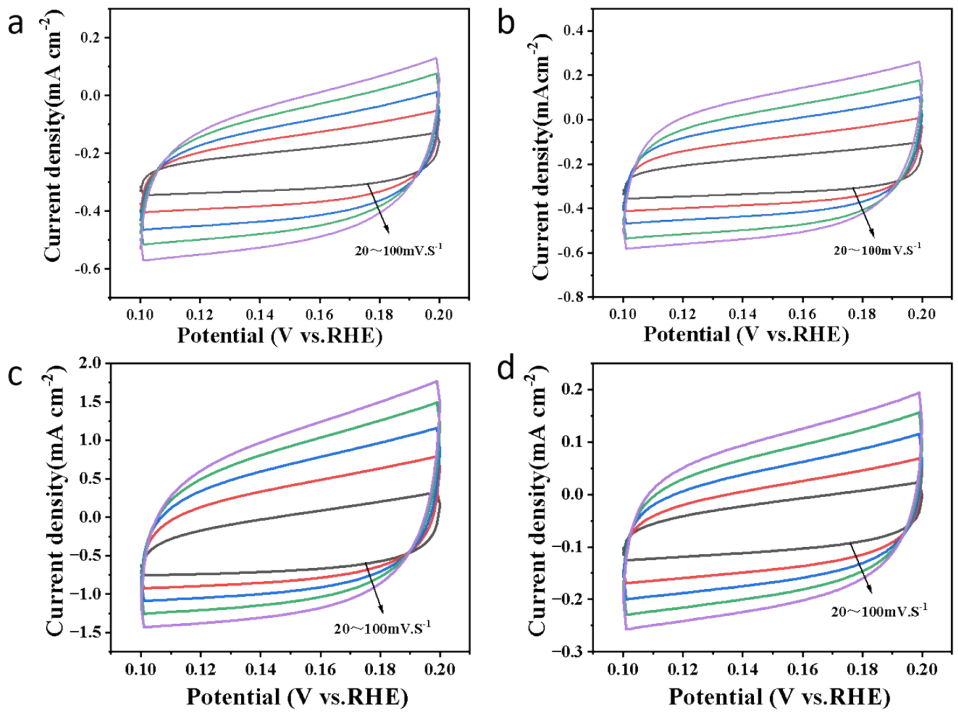

Fig. S10. OER-CV of (a) W-CoO/NF (b) W-CoSe200/NF (c) W-CoSe300/NF and (d) W-CoSe400/NF at different sweep speeds.

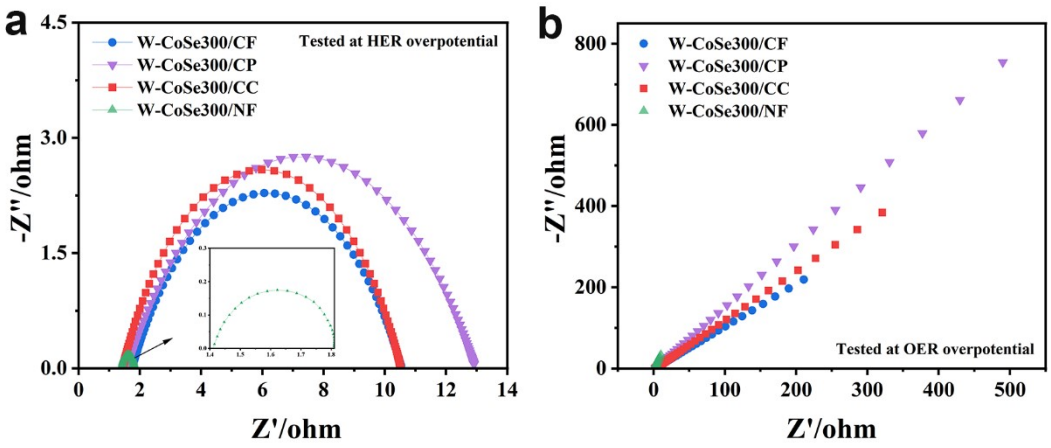

Fig. S11. EIS Nyquist plots of W-CoSe300 electrocatalysts loaded on different conductive substrates.

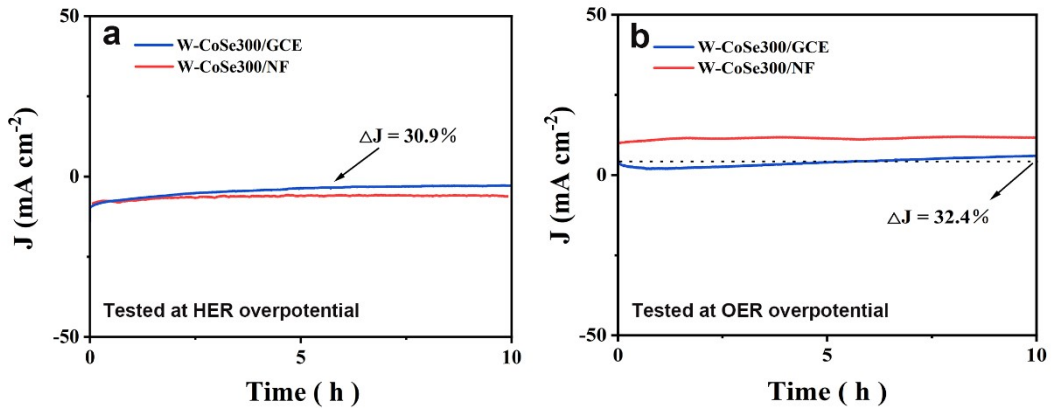

Fig. S12. Stability tests of W-CoSe300/GCE and W-CoSe300/NF electrocatalysts under HER and OER overpotentials (GCE = glassy carbon electrode).

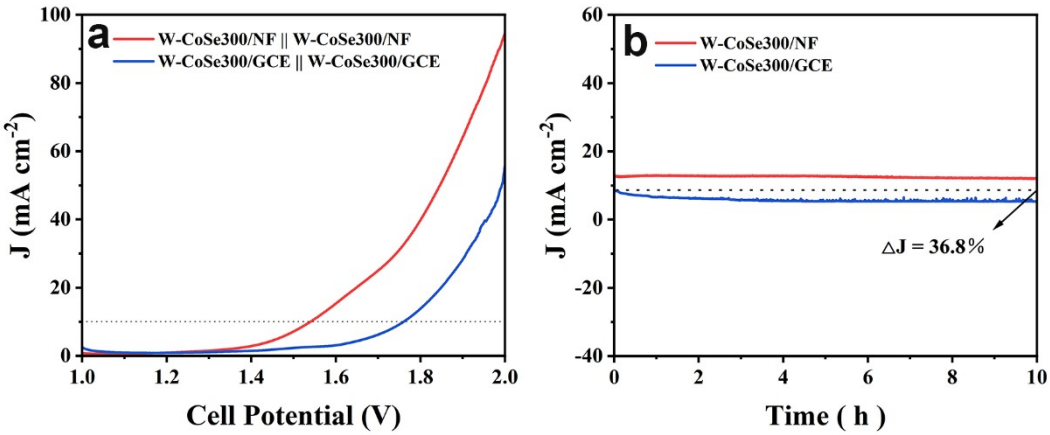

Fig. S13. OWS performance of W-CoSe300/GCE (GCE = glassy carbon electrode) and W-CoSe300/NF electrocatalysts: (a) LSV curves, (b) electrochemical stability test.

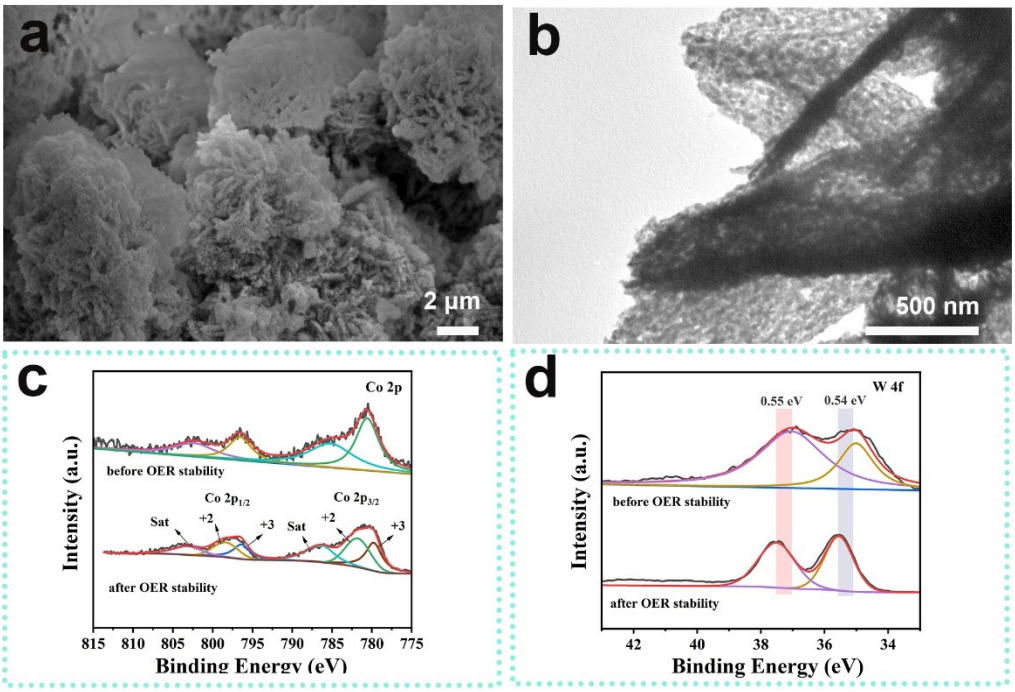

Fig. S14. Characterization analysis of the W-CoSe300/NF electrocatalyst after OER stability testing: (a) SEM image, (b) TEM image, (c, d) XPS spectra.

Table S1. The comparison for HER performance of W-CoSe300/NF synthesized in this work and recently reported catalysts.

Catalyst electrodes	Electrolyte	Overpotential @50 mA cm^{-2} （mV）	Ref.
W-CoSe300	**1.0 M KOH**	**84**	**This work**
RhNiFe	1.0 M KOH	36	[1]
FeMo/MoC@C	1.0 M KOH	201	[2]
CoFeP/NF	1.0 M KOH	350	[3]
N-NiCoP/NF	1.0 M KOH	119	[4]
Co-NiS @ MoS_2	1.0 M KOH	139.9	[5]
Zn_3N_2–Co_2N	1.0 M KOH	121.7	[6]
NiFe-MS/MOF@NF	1.0 M KOH	156	[7]
Co-Ni_2P	1.0 M KOH	116	[8]
Ni_3S_2@NiSe/NF	0.5 M H_2SO_4	289	[9]
Co-Mo-P/Co-Zn-S	1.0 M KOH	165	[10]

Table S2. The comparison for OER performance of W-CoSe300/NF synthesized in this work and recently reported catalysts.

Catalyst electrodes	Electrolyte	Overpotential @50 mA cm^{-2} （mV）	Ref.
W-CoSe300	**1.0 M KOH**	**283**	**This work**
CoP–N/Co foam	1.0 M KOH	260	[11]
$Co_{0.85}Se$@Co foam	1.0 M KOH	360	[12]
CFL-200	1.0 M KOH	266	[13]
Co@NC	1.0 M KOH	452	[14]
$Co_{0.8}Fe_{0.2}$–Mo_2C-80	1.0 M KOH	246.5	[15]
$FeCo_2S_4$/NF	1.0 M KOH	270	[16]
Co-MOF/NF	1.0 M KOH	266	[17]
SS NAC P-400	1.0 M KOH	220	[18]
NiCoFe/NF	1.0 M KOH	233	[19]
CH@PBA-P/CF	1.0 M KOH	312	[20]

Table S3. The comparison for overall water splitting (OWS) performance of W-CoSe300/NF synthesized in this work and recently reported catalysts.

Catalyst electrodes	Electrolyte	$E_{j=10}$ (V)	Durability (h)	Ref.
W-CoSe300	**1.0 M KOH**	**1.54**	**120**	**This work**
MOF-V-Ni_3S_2/NF	1.0 M KOH	1.58	10	[21]
$Co_{0.4}Mo_{0.6}P$@CL-NCNF	1.0 M KOH	1.59	24	[22]
CoSe@NiFe	1.0 M KOH	1.53	12	[23]
CoFeRu@C	1.0 M KOH	1.59	12	[24]
CoOSeP@Co foil	1.0 M KOH	1.74	30	[25]
DLC FCP@NG	1.0 M KOH	1.63	30	[26]
Fe-P-CMO	1.0 M KOH	1.48	60	[27]
F-CoO	1.0 M KOH	1.53	60	[28]
Ru-NiCoP/NF	1.0 M KOH	1.515	50	[29]
J-CoFe-CFP	1.0 M KOH	1.56	10	[30]

1. K. Karthick, A. B. Mansoor Basha, A. Sivakumaran and S. Kundu, *Catalysis Science & Technology*, 2020, **10**, 3681-3693.
2. H. Li, T. Wang, M. Xu, P. Wang, Z. Gao, W. Zhang, M. Liu and M. Feng, *Journal of Alloys and Compounds*, 2024, **987**, 174199.
3. C. Zhang, W. Wang, P. He, R. Hu, L. Ran, Y. Li and J. Yan, *New Journal of Chemistry*, 2023, **47**, 737-742.
4. Y. Liu, Z. Li, H. Sun, L. Zheng, Z. Yuan, S. Li, Y. Li, X. Fang, Y. Gao, Z. Wang, X. Dai, X. Zhang and W. Song, *Journal of Materials Chemistry A*, 2023, **11**, 1256-1267.
5. H. Gao, J. Zang, Y. Wang, S. Zhou, P. Tian, S. Song, X. Tian and W. Li, *Electrochimica Acta*, 2021, **377**, 138051.
6. D. C. Nguyen, T. L. Luyen Doan, X. Zhu, N. H. Kim and J. H. Lee, *Journal of Materials Chemistry A*, 2023, **11**, 25332-25344.
7. M. Zhao, W. Li, J. Li, W. Hu and C. M. Li, *Advanced Science*, 2020, **7**, 2001965.
8. X. Sun, P. Yang, S. Wang, J. Hu, P. Chen, H. Xing and W. Zhu, *International Journal of Hydrogen Energy*, 2022, **47**, 28495-28504.
9. N. Shaikh, I. Mukhopadhyay and A. Ray, *Journal of Materials Chemistry A*, 2022, **10**, 12733-12746.
10. M. Shamloofard and S. Shahrokhian, *Nanoscale*, 2021, **13**, 17576-17591.
11. Z. Liu, X. Yu, H. Xue and L. Feng, *Journal of Materials Chemistry A*, 2019, **7**, 13242-13248.
12. H. Yang, L. Jiang, J. Yan, L. Zhang and Q. Liang, *Journal of Materials Science: Materials in Electronics*, 2020, **31**, 9385-9393.
13. S. Wang, F. Yuan, G. Yang, S. Luo, M. Chen, T. Fan and J. Ma, *Molecular Catalysis*, 2022, **525**, 112339.
14. S. G. Peera, R. Koutavarapu, C. Liu, G. Rajeshkhanna, A. Asokan and C. V. Reddy, *Journal*, 2021, **14**.
15. M. S. A. Sher Shah, H. Jung, V. K. Paidi, K.-S. Lee, J. W. Han and J. H. Park, *Carbon Energy*, 2024, **n/a**, e488.
16. J. Hu, Y. Ou, Y. Li, D. Gao, Y. Zhang and P. Xiao, *ACS Sustainable Chemistry & Engineering*, 2018, **6**, 11724-11733.
17. Z. Huang, L. Hao, X. Ma, S. Zhang, R. Zhang, K. Yue and Y. Wang, *Inorganic Chemistry*, 2021, **60**, 4047-4057.
18. Q. Zhou, J. Jia, G. Huang and C. Feng, *New Journal of Chemistry*, 2023, **47**, 6645-6652.
19. C. Su, D. Wang, W. Wang, N. Mitsuzaki, R. Shao, Q. Xu and Z. Chen, *Journal of Electroanalytical Chemistry*, 2024, **960**, 118167.
20. J. Chen, Y. Li, H. Ye, P. Zhu, X.-Z. Fu and R. Sun, *Dalton Transactions*, 2022, **51**, 13451-13461.
21. W. Dong, H. Zhou, B. Mao, Z. Zhang, Y. Liu, Y. Liu, F. Li, D. Zhang, D. Zhang and W. Shi, *International Journal of Hydrogen Energy*, 2021, **46**, 10773-10782.
22. T. Huang, G. Xu, H. Ding, L. Zhang, B. Wei and X. Liu, *Journal of Colloid*

and Interface Science, 2022, **625**, 956-964.
23. H. Sun, J.-G. Li, L. Lv, Z. Li, X. Ao, C. Xu, X. Xue, G. Hong and C. Wang, *Journal of Power Sources*, 2019, **425**, 138-146.
24. M. Yang, T. Feng, Y. Chen, J. Liu, X. Zhao and B. Yang, *Applied Catalysis B: Environmental*, 2020, **267**, 118657.
25. Y.-F. Jiang, C.-Z. Yuan, X. Zhou, Y.-N. Liu, Z.-W. Zhao, S.-J. Zhao and A.-W. Xu, *Electrochimica Acta*, 2018, **292**, 247-255.
26. Y. Lu, Y. Chen, K. Srinivas, Z. Su, X. Wang, B. Wang and D. Yang, *Electrochimica Acta*, 2020, **350**, 136338.
27. B. Wang, X. Chen, Y. He, Q. Liu, X. Zhang, Z. Luo, J. V. Kennedy, J. Li, D. Qian, J. Liu and G. I. N. Waterhouse, *Applied Catalysis B: Environment and Energy*, 2024, **346**, 123741.
28. C. Zhong, Z. Han, T. Wang, Q. Wang, Z. Shen, Q. Zhou, J. Wang, S. Zhang, X. Jin, S. Li, P. Wang, D. Gao, Y. Zhou and H. Zhang, *Journal of Materials Chemistry A*, 2020, **8**, 10831-10838.
29. D. Chen, R. Lu, Z. Pu, J. Zhu, H.-W. Li, F. Liu, S. Hu, X. Luo, J. Wu, Y. Zhao and S. Mu, *Applied Catalysis B: Environmental*, 2020, **279**, 119396.
30. X. Li, H. Zhang, X. Li, Q. Hu, C. Deng, X. Jiang, H. Yang and C. He, *Nano Research*, 2023, **16**, 2245-2251.